



ORIGINAL RESEARCH ARTICLE

# Yttrium-Stabilized Zirconia Ceramics Fabrication through Material Extrusion 3D Printing

*Xiuhu Guo, Chuanyong Li, Lu Li, Zhentao Yuan, Xiao Wang, Weichen Zhang, Junnan Liu, Gang Chen, Xiaoying Cui, and Yaoping Xu*

Submitted: 12 September 2023 / Revised: 2 April 2024 / Accepted: 2 May 2024

**In this study, the authors refined and molded 8 wt.% yttrium-stabilized zirconia (8YSZ) ceramic powders by using extrusion 3D printing to obtain green bodies. The green bodies were then subjected to degreasing and sintering to obtain the final parts. It used two printing nozzles, with diameters of 0.8 and 0.6 mm, for 3D molding, and examined the macroscopic and microscopic characteristics of the green, brown, and sintered parts. The parts printed by using both nozzles exhibited smooth surfaces and satisfactory layer-to-layer bonding. However, there were differences in the densities of the sintered parts obtained by using the two nozzles. The sintered part printed by using the nozzle with a diameter of 0.6 mm had a higher density of 5.37 g/cm<sup>3</sup>, while that printed by using the nozzle with a diameter of 0.8 mm had a density of 4.59 g/cm<sup>3</sup>. The bending strengths of the sintered bodies manufactured by using nozzles with diameters of 0.8 and 0.6 mm were 114.4 and 261.9 MPa, respectively.**

**Keywords** 8YSZ, 3D printing, agglomerant, mechanical properties, printing parameters

## 1. Introduction

Three-dimensional (3D) printing technology is a technique of fabrication that eliminates the need for conventional methods of manufacturing. By applying the principle of “layer-by-layer deposition,” it can be used to sequentially stack 2D *x-y* planes to create intricate 3D structures that are challenging to construct by using traditional processes. This approach allows for the creation of complex structural designs, and facilitates the integration of material and structure as well as structure and function (Ref 1-3). In contrast, traditional methods of manufacturing involve subtractive techniques in which an excessive amount of material is removed from the workpiece to obtain components of the desired shape and size. Moreover, conventional approaches suffer from such drawbacks as poor efficiency of use of materials and long production cycles (Ref 4, 5).

Ceramics have high mechanical strength and hardness, low thermal conductivity, high abrasion and corrosion resistance,

and are therefore widely used as heat-insulating tiles for spacecraft, solid oxide fuel cells, heat-insulating materials for automobile engines, and in the dental field. (Ref 6-9). Zirconia ceramics exhibit a monoclinic structure at room temperature that is transformed into tetragonal and hexagonal structures at higher temperatures (Ref 10, 11). These ceramics offer a high flexural strength, thermal and chemical stability, suitable biocompatibility, and corrosion resistance (Ref 12-14). Due to these characteristics, zirconia ceramics in general, and yttrium-stabilized zirconia (YSZ) ceramics in particular, have garnered significant attention in industrial and medical applications (Ref 15, 16). However, compared with the 3D printing of plastics and metals, the additive manufacturing of ceramics faces considerable challenges in terms of balancing the reliability of their performance, their cost, and their surface quality (Ref 17). Grossin (Ref 18) used powder bed selective laser processing (sintering/melting) to fabricate the ceramics silicon carbide, zirconia, and alumina. He compared the use of direct and indirect methods of powder bed selective laser processing for fabricating each ceramic, and highlighted outstanding issues in their processing. Shishkovsky (Ref 19) used laser melting technology to manufacture parts made of zirconia, and examined the presence of such defects as cracks and voids in them. Manufacturing completely dense ceramics directly through selective laser sintering (SLS) or selective laser melting (SLM) what is now known as directed energy deposition (DED) in the context of 3D printing poses challenges owing to their high melting point and low rate of diffusion (Ref 20, 21).

The 3D printing of ceramic parts by using material extrusion (MEX) has the advantages of low cost, simplicity of operation, and energy efficiency (Ref 22). The mold in this process is formed by rotating the screw to melt the granular feed into the filament while using pressure from a gas to drive the piston (Ref 23). The technology for the MEX of ceramics by using an organic binder along with a ceramic as raw material has promising prospects for application as it benefits from the maturity of ceramic injection molding (CIM) technology (Ref

**Xiuhu Guo, Chuanyong Li, Lu Li, Weichen Zhang, and Junnan Liu**, Faculty of Material Science and Engineering, Kunming University of Science and Technology, Kunming 650093, People's Republic of China; **Zhentao Yuan** and **Xiao Wang**, City College, Kunming University of Science and Technology, Kunming 650051, People's Republic of China; **Gang Chen**, Institute for Advanced Materials and Technology, University of Science and Technology Beijing, Beijing 100083, People's Republic of China; **Xiaoying Cui**, Research Center for Analysis and Measurement, Kunming University of Science and Technology, Kunming 650093, People's Republic of China; and **Yaoping Xu**, Yunnan Titanium Industry Co., Chuxiong 651200, People's Republic of China. Contact e-mails: liluchina@kust.edu.cn and 1572833461@qq.com.

24). Nötzel (Ref 25) proposed a ratio of raw materials for the preparation of alumina wires with a high solid loading (55 vol.%), and used it to obtain 3D-printed parts with a high surface quality by using MEX technology. Furong (Ref 26) prepared dense  $\text{Si}_3\text{N}_4$  ceramics without prominent defects through fused deposition modeling combined with sintering by using gaseous pressure. This study also characterized the steps on the surface of the ceramic, interlayer bonding, and the evolution of its microstructure. Rane (Ref 27) used mature technology for the injection molding of ceramics to prepare dense 3D zirconia ceramics with a uniform structure and a smooth surface through laser melting deposition.

In this study, using 8YSZ particles, the authors investigated the relationship between the flow of two nozzle diameters and the binder and printing parameters by applying material extrusion 3D printing techniques. By continuously improving the process, we obtained a better set of binder formulations, printing parameters, degreasing and sintering processes for extrusion 3D printing of ceramic materials, which resulted in printed parts with uniform shaping and strength. It also compared the surface morphology, microstructure and mechanical properties of parts printed using different nozzle diameters to verify the feasibility of material extrusion 3D printing of 8YSZ ceramics.

## 2. Materials and Methods

### 2.1 Experimental Materials

Zirconia and yttrium oxide powders that were extruded from fused deposition powder were supplied by Suzhou Yuante New Materials Co., Ltd. ( $D_{50}$  was 200 nm). The organic binder was mainly composed of 60% (mass fraction) paraffin wax (PW, Sinopec), 20% ethylene-vinyl acetate copolymer (EVA, U1649, USI), 15% polyethylene (PE, TR480, Sinopec), and 5% stearic acid (SA, Sinopec). The 8YSZ powder and binder were first mixed at 140 °C for 60 ~ 80 min by using a twin-roll mixer (Wuhan Qien Technology Development Co., Ltd.) to mix them evenly. The 8YSZ feed was then crushed by a crusher (Shanghai Youxing Electromechanical Co., Ltd.). The diameter of the particles after the feed had been crushed was the range of in 3-5 mm, and the solid loading of 8YSZ was 45 vol.%.

### 2.2 Experimental Method

The process of material extrusion (MEX) of the 8YSZ ceramics is shown in Fig. 1.

The yttrium oxide and zirconia powders were proportionally ball-milled, with alcohol as the medium, by using a planetary ball mill. The slurry obtained after ball milling was dried in a drying oven. Following this, the 8YSZ raw material was mixed with the organic binder by using a twin-roll mixer. After having been cooled, it was broken to obtain a homogeneous feed of the 8YSZ ceramic. The 8YSZ feedstock was added to the melt-deposited 3D printer hopper, and was transported by a screw to a barrel coated with a heating coil. The solid 8YSZ feedstock was melted into a liquid-solid mixture with good fluidity through heating by using the coil. The feed and nozzle used for 3D printing are shown in Fig. 2. The molten wire was stacked in a layer-by-layer fashion through the continuous extrusion of the screw to form 8YSZ green billets with a variety of complex shapes. Finally, the green bodies were degreased by using an n-

hexane solvent, thermally degreased, and sintered to obtain sintered 8YSZ bodies.

### 2.3 Material Testing and Characterization

The 3D-printed feedstock was thermally decomposed for thermogravimetric analysis (TGA, STA449F3, NETZSCH) to examine the range of temperature of the thermal debinding and sintering of the printed green body. The heating rate was 10 °C/min and the test atmosphere was argon. The densities of the green body and the sintered body were measured by using the Archimedes drainage method. The phase analysis of the sintered body was carried out by using an x-ray diffractometer (XRD). The test conditions were as follows: The source of radiation was  $\text{Cu-K}\alpha$ ,  $\lambda = 0.15406$  nm, the tube voltage was 20 kV, the tube current was 30 mA, the scanning speed was 0.03° /s, and the range of  $2\theta$  scanning was 20° ~ 80°. A tungsten-filament scanning electron microscope (SU3900, Hitachi Hi-Tech, Japan) was used to observe the surface and interlayer microstructure of the 3D-printed 8YSZ green bodies and sintered bodies.

We used the GB/T6569-2006 method to test the bending strength of the 3D-printed 8YSZ ceramics by using an electronic universal testing machine (CMT6103, MTS). The dimensions of the sample were 2 × 7 × 60 mm. The testing parameters had a span of 30 mm, and the loading rate was 0.5 mm/min. A diagram of the simulation is shown in Fig. 3.

## 3. Results and Discussion

### 3.1 Relationship Between Stability of Flow of Extrudate from Nozzle and Proportion of Binder

The temperature of the barrel during printing can influence the viscosity of the feed and, thus, the fluidity of extrusion from the nozzle. When printing by using a nozzle with a diameter of 0.8 mm, the contents of the components of the adhesive were 60 PW, 20 EVA, 15 PE, and 5 wt.% SA. The temperature of the barrel was 140 °C, the rate of flow of the liquid-solid mixture extrusion tended to be stable, and the molding was more uniform. When printing by using a nozzle with a diameter of 0.6 mm, the contents of components of the adhesive were 65 PW, 15 EVA, 15 PE, and 5 wt.% SA. The temperature of the barrel was 130 °C, and this yielded printed parts with a uniform molding and strength. Figure 4 shows the parts printed by using the two nozzles with different diameters. It is clear from it that the flow of the extrudate from the nozzle was uniform during the printing process, the line was clean and tidy, and no accumulation at the nozzle or burr on the printed parts was observed.

### 3.2 Molding, Degreasing, and Sintering for 3D Printing

The parameters of 3D printing were as follows. The speed of printing was 40 mm/s, the temperature of the nozzle was 130 ~ 140 °C, the temperature of the hot bed was 100 °C, and the height of each layer was 0.2 mm. The 3D-printed 8YSZ green body was subsequently placed in an n-hexane solution in a water bath at 40 °C for 20 h for degreasing, and was then dried in a drying oven at 50 °C for 12 h. The degreasing process is shown in Fig. 5(a). Following degreas-

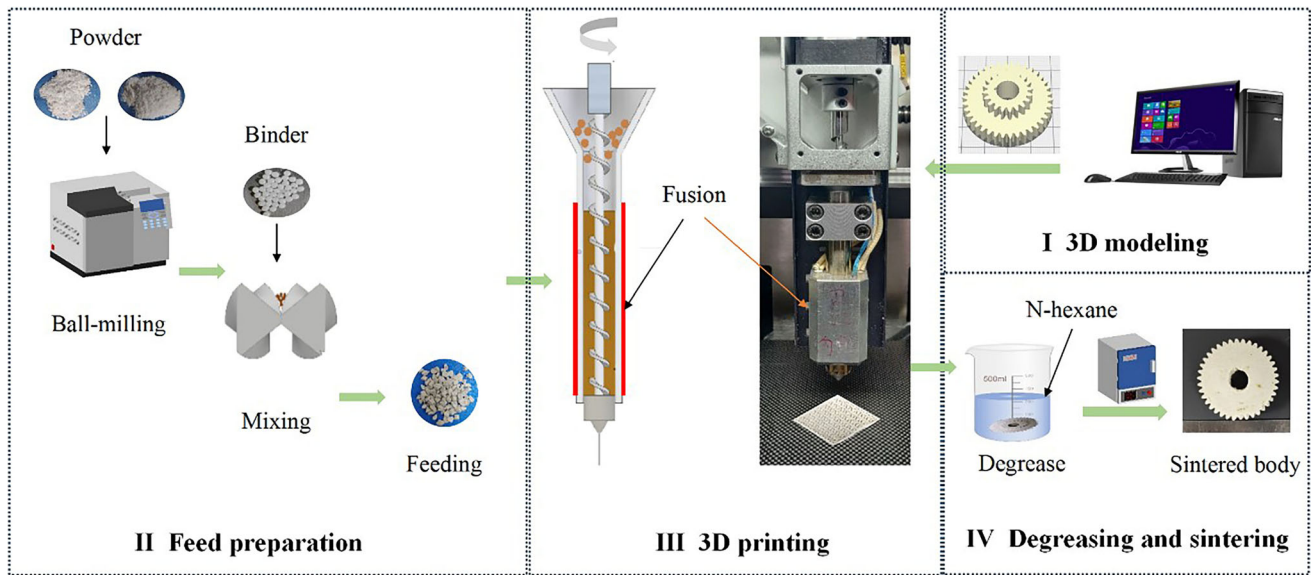


**Fig. 1** 8 Process flow diagram of YSZ ceramic fused deposition 3D printing

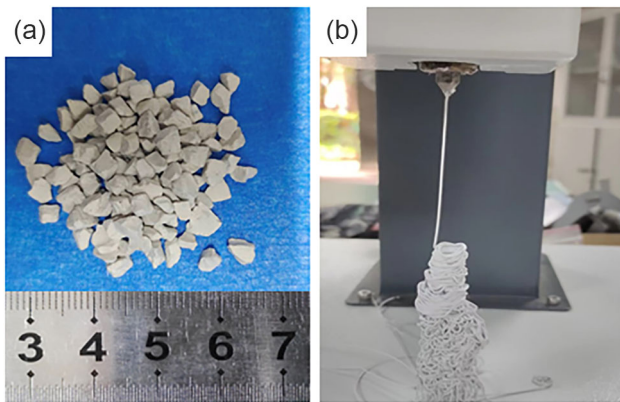
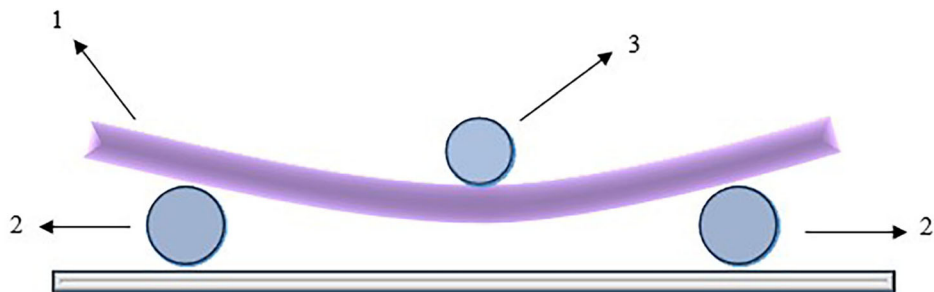


**Fig. 2** (a) 8YSZ 3D printing feed; (b) Melt spinning situation

ing and drying with the n-hexane solvent, the rate of degreasing of the printed green body was 93 ~ 97%, which proved that its PW component had been removed. According to the TG-DSC curve of the feed shown in Fig. 5(b), the printing feed yielded exothermic peaks at about 90 110 1350, and 460 °C, but the curve of TG showed that the quality of the feed had not significantly degraded before reaching a temperature of 300 °C. This result might have been obtained due to the evaporation of water or organic solvents in this range of temperature. The TG curve exhibited two prominent stages of decline at 350 and 460 °C, which showed that the organic binder had undergone thermal decomposition at this time. Therefore, it was necessary to maintain the temperature in this range for a long time in order to remove as much of the organic binder as possible. It is also necessary to control the rate of heating to prevent the green body from cracking



The two sticks on the outside can roll freely to the outside, and the sticks in the middle can not roll.

- 1 — Test specimen;
- 2 — Rollable rollers;
- 3 — Rollable loading indenter.

**Fig. 3** Bending resistance test of 3D printed ceramic parts



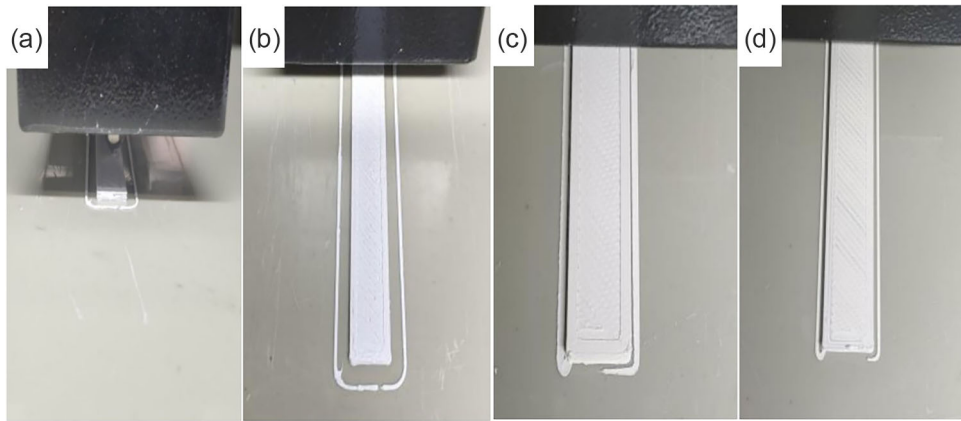


**Fig. 4** (a, b) are 0.8 mm nozzle prints; (c, d) are 0.6 mm nozzle printing parts

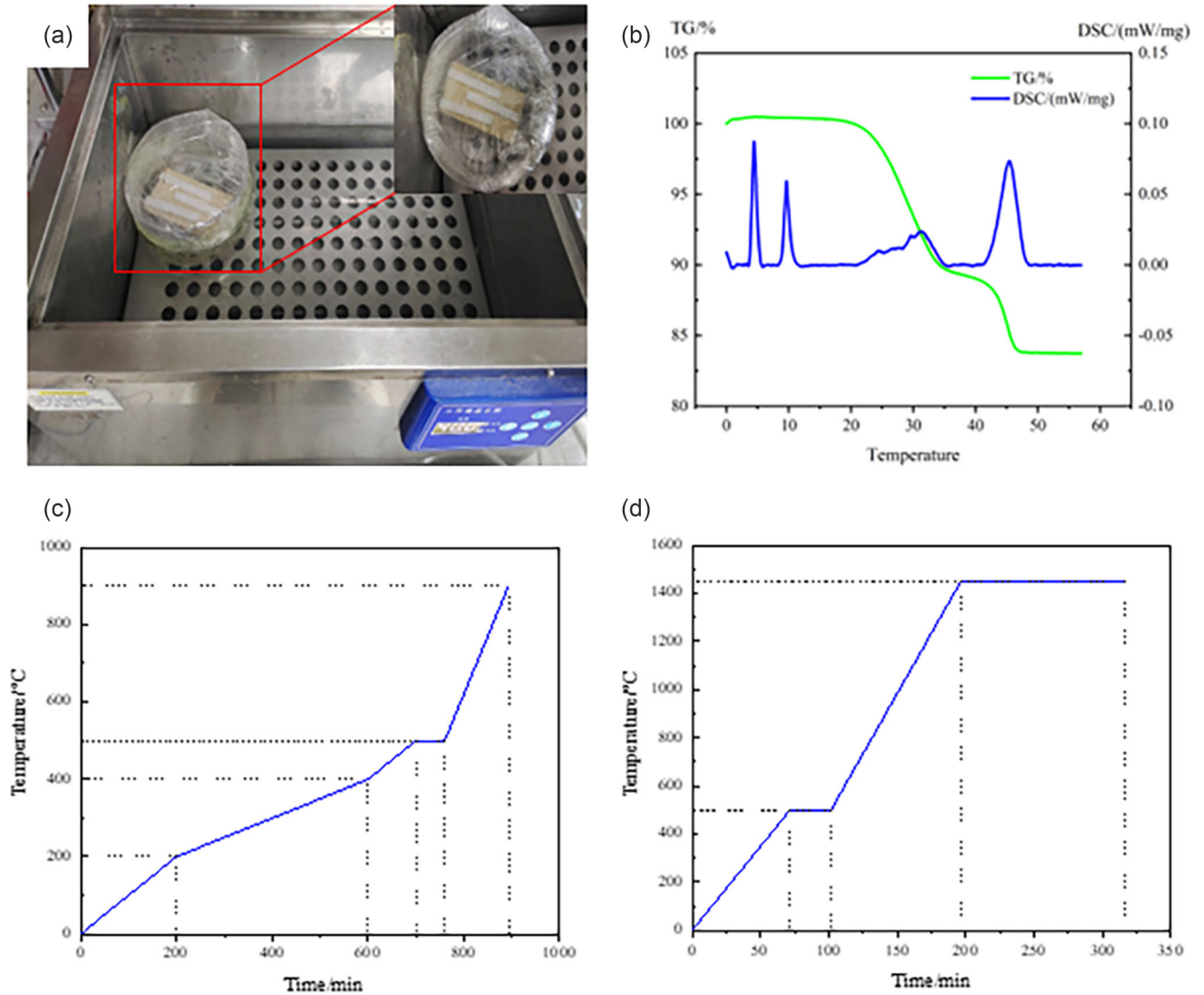


**Fig. 5** (a) n-hexane water bath degreasing diagram; (b) TG-DSC curve of 3D printing feedstock; (c) Printing the thermal debinding and pre-sintering curves of the green body; (d) Sintering process of 3D printed parts

owing to excessively fast degreasing. The thermal debinding of the sample and its curve of sintering are shown in Fig. 5(c) and (d).

After the thermal degreasing and pre-sintering of the printed parts, the muffle furnace was heated to 900 °C to greasing curve of the process shown in Fig. 5(c), and was then cooled.

The pre-sintering temperature was 900 °C, and caused the green body to gain strength. The sample was then placed in a sintering furnace, heated to 1,450 °C at the rate shown in Fig. 5(d), and was maintained at 1,450 °C for 2 h and then left to cool in the furnace.

### 3.3 SEM Images of Powders and Printed Parts

**3.3.1 The 8YSZ Raw Materials for 3D Printing.** The patterns of the XRD analyses of yttrium oxide and zirconia powder are shown in Fig. 6(a) and (b), from which it was clear that there was no peak of impurity in either. The scanning diagram and EDS elemental analysis of the 8YSZ powder obtained after ball milling are shown in Fig. 6(c) and (d). The EDS energy spectrum showed that the distribution of yttrium and zirconium was rendered uniform through ball milling, and satisfactorily yielded yttrium-stabilized zirconia. The 8YSZ ceramic powder for 3D printing was thus obtained, and was then mixed with the binder at a certain volumetric ratio to obtain the printing feed, as shown in Fig. 2(a).

**3.3.2 The 3D Printing of 8YSZ Parts.** The 3D printing is a process of layer-by-layer stacking on a set plane. The surface quality and interlayer bonding of the molded sample are key factors influencing the effectiveness of the process. The surface quality is directly related to the accuracy with which the

surface is molded and the cost of its subsequent processing, while the interlayer bonding influences the mechanical properties of the sintered body. Figure 7(a) and (b) shows images of scans of the surface and sides of the printed parts when the nozzle with a diameter of 0.8 mm was used and the temperature of the barrel was 140 °C. Figure 7(c) and (d) shows images of scans of their surface and sides when the nozzle with a diameter of 0.6 mm was used and the temperature of the barrel was 130 °C. The height of the printing layer was set to 0.2 mm. Following the printing of one layer, the platform was lowered by 0.2 mm and a new layer was printed. The thickness of each layer was controlled by lowering the printing platform. The surfaces of parts printed by using the two nozzles were smooth, the side layers were clear, and the bonding was tight. This proved that the wire extruded by using the printing nozzle was dense and uniform.

After thermal debinding as determined by the TG-DSC curve, the ceramic parts were sintered to 1,450 °C and maintained at this temperature for 2 h according to the sintering process. The interlayer scanning images of parts printed by using nozzles with diameters of 0.8 and 0.6 mm are shown in Fig. 8. A small gap was observed at the interface after sintering, and was formed due to shrinkage after degreasing and sintering (the rate of linear shrinkage was 22 ~ 25%, as shown in Fig. 10). However, no prominent gap was observed in most

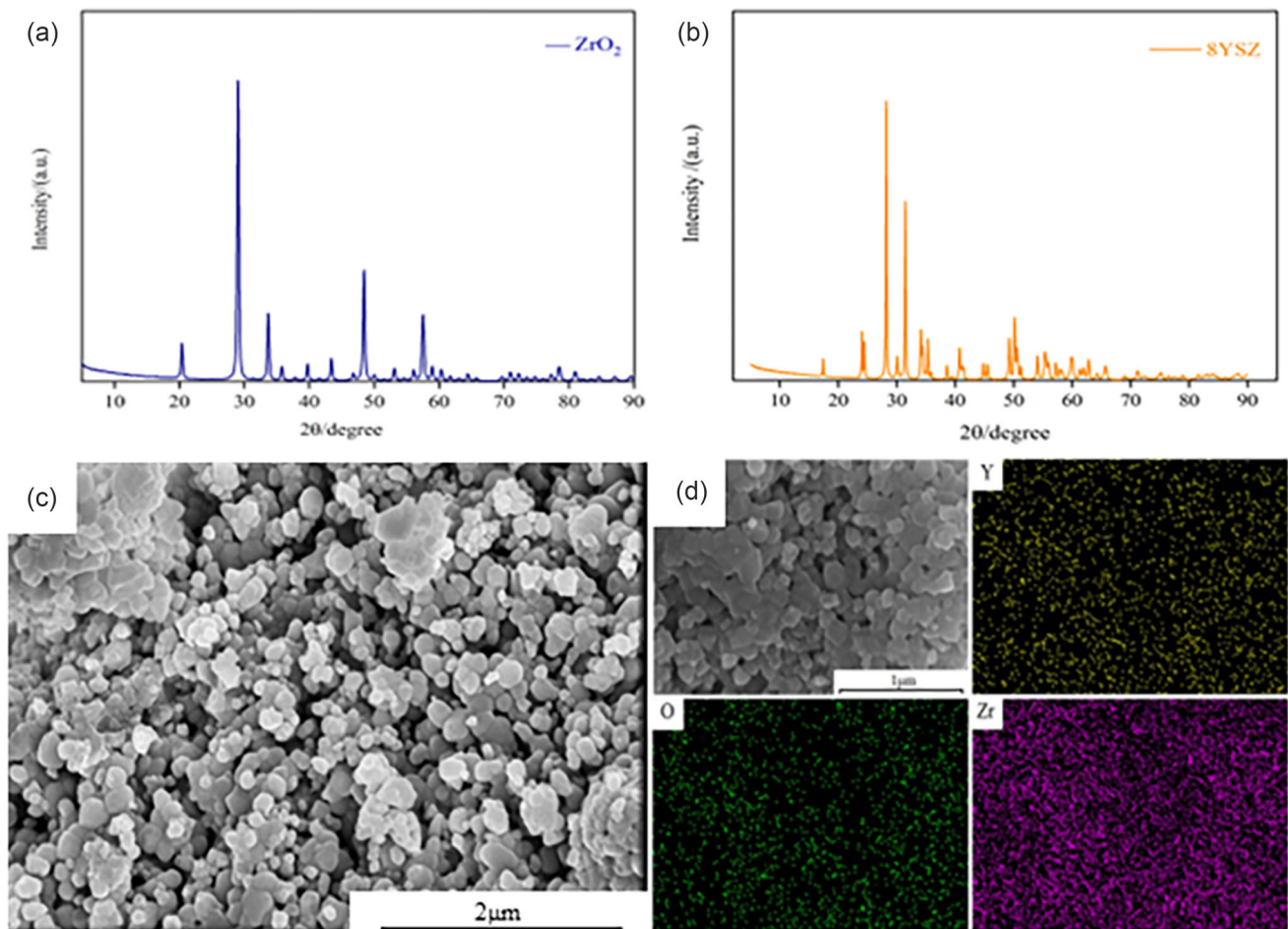


**Fig. 6** (a, b) are the XRD spectra of ZrO<sub>2</sub> and 8YSZ, respectively; (c, d) SEM images of 8YSZ powder after ball milling and energy spectral images of the distribution of each element of the powder, respectively



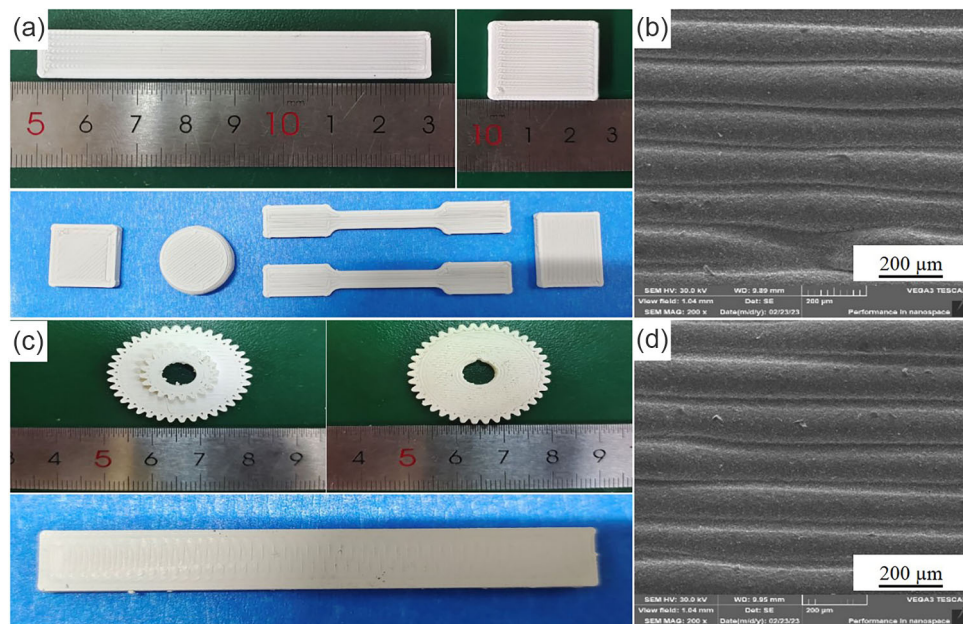


**Fig. 7** (a, b) Interlayer scanning images of 0.8 mm nozzle printed parts and green blanks; (c, d) 0.6 mm nozzle prints and green layer scanning diagram

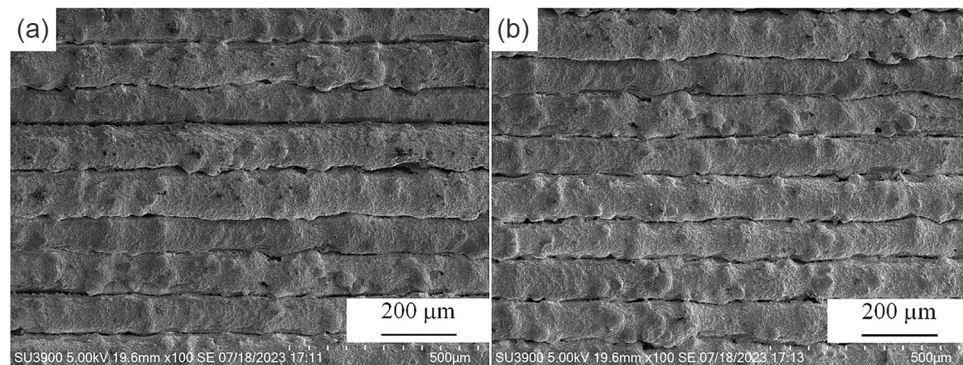


**Fig. 8** (a, b) respectively 0.8 and 0.6 mm nozzle printing sintered body layer SEM images

areas, and the microstructure of the middle layer was as dense and uniform as that of the inner layer.

A map of the internal scan of the sintered body is shown in Fig. 9. We compared the scanning maps of the sintered bodies based on parts obtained by nozzles with diameters of 0.8 and 0.6 mm. The density of the part printed by using the nozzle with a diameter of 0.8 mm was  $4.59 \text{ g/cm}^3$  while that of the part printed by using the nozzle with a diameter of 0.6 mm was  $5.37 \text{ g/cm}^3$ . The density of the latter part was 89.8% of the theoretical density of the 8YSZ ceramic (Ref 23). We also obtained ratios of the binder corresponding to the two nozzles such that both could be stably and evenly discharge the extrudate. The results showed that the nozzle with a diameter of 0.8 mm was preferable when printing porous or hollow ceramic parts, while that with a diameter of 0.6 mm should be used for ceramic parts with particular porosity-related requirements or denser ceramic parts.

### 3.4 Mechanical Properties

The sintered 8YSZ body used for the test of bending strength is shown in Fig. 10. To provide a sound experimental

basis for the subsequent analysis of the reliability of the samples, we used 10 samples each prepared by using the two nozzles with different diameters to test their mechanical properties.

The results of the test of bending strength are shown in Table 1. The mechanical properties of the parts printed by using the nozzle with a diameter of 0.6 mm were stable at around 261 MPa. The sample was then subjected to three sets of nanoindentation tests. The Vickers hardness of the ceramic parts was about 1510 HV. This shows that parts of the 8YSZ ceramic printed by using the nozzle with a diameter of 0.6 mm were harder than those formed by other methods of 3D printing (Ref 28).

## 4. Conclusions

In this study, the optimal ratio and parameters were determined through continuous testing and the 8YSZ ceramic parts were successfully printed. The printed parts achieved a

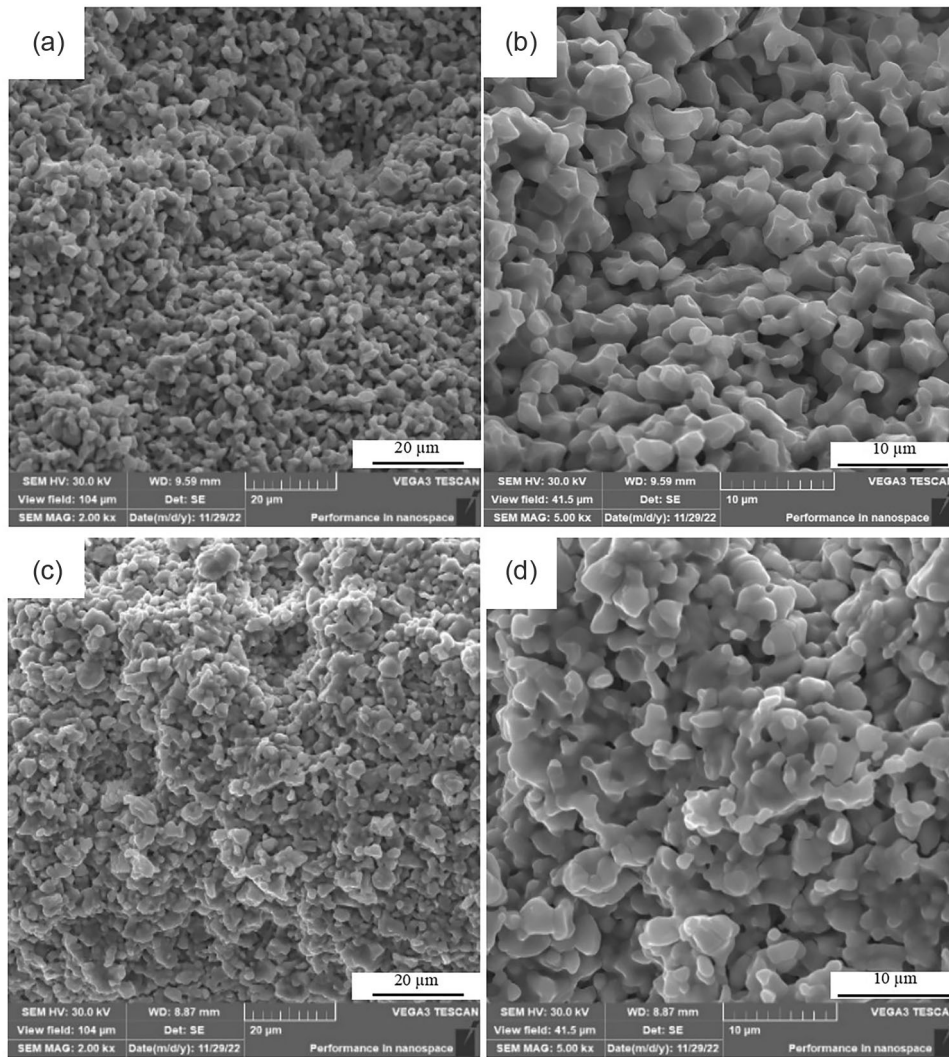


**Fig. 9** (a, b) is 0.8 mm printing sintered body SEM diagram; (c, d) is 0.6 mm printing sintered body SEM images

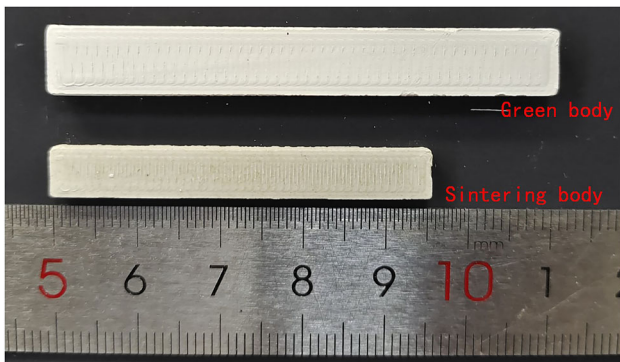


**Fig. 10.** 8YSZ sintered body for bending test

Vickers hardness of 1510 HV and a maximum bending strength of 261.9 MPa.

- (1) It determined two proportional compositions of adhesive corresponding to nozzles with diameters of 0.6 and 0.8 mm for printing. By adjusting the proportion of the binder, we obtained a feed that allowed stable printing.
- (2) It determined the parameters of material extrusion for 3D printing of 8YSZ ceramic parts. This allowed us to print uniform and stable parts by using nozzles of different diameters, while ensuring precise control of the flow of the extrudate and dense bonding between layers of part.

**Table 1** Mechanical properties of two different nozzle prints

	Flexural modulus, MPa	Bending strength, MPa	Width, mm	Thickness, mm
0.8 mm	17584.77	114.4	7.68	2.13
0.6 mm	73958.95	261.9	7.77	2.1



- (3) It determines the degreasing and sintering process of 8YSZ ceramic parts for 3D printing. The flexural strength of the sintered body obtained using a nozzle with a diameter of 0.6 mm was approximately 261.9 MPa.

## Acknowledgment

The authors would like to gratefully acknowledge the support of Key Research and Development Project of Yunnan Province and International Science and Technology Cooperation Project (202103AF140004), Technology talent and platform plan (202305AQ350001), Key research and development project of Yunnan Province (202203AM140010). This work is supported by the National and Local Joint Engineering Laboratory of Advanced Metal Solidification Forming and Equipment Technology, and Joint Laboratory for Key Technologies of Titanium Forming, Kunming University of Science and Technology, Kunming, China.

## References

1. A. Atala, Introduction: 3D Printing for Biomaterials, *Chem. Rev.*, 2020, **120**, p 10545–10546.
2. B. Aktas, S. Tekeli, and S. Salman, Synthesis and Properties of La2O3-Doped 8 mol.% Yttria-Stabilized Cubic Zirconia, *J. Mater. Eng. Perform.*, 2013, **23**, p 294–301.
3. B. Aktas, S. Tekeli, and S. Salman, Improvements in Microstructural and Mechanical Properties of ZrO2 Ceramics after Addition of BaO, *Ceram. Int.*, 2016, **42**, p 3849–3854.
4. X. Zhang, Q. Yang, L. Chen, P. Song, and J. Feng, Fabrication and Characterization of 8YSZ Ceramic based Abradable Seal Coatings by Atmospheric Plasma Spraying, *Ceram. Int.*, 2020, **46**, p 26530–26538.
5. S. Tekeli, M. Erdogan, and B. Aktas, Influence of  $\alpha$ -Al2O3 Addition on Sintering and Grain Growth Behaviour of 8 mol.% Y2O3-Stabilised Cubic Zirconia (c-ZrO2), *Ceram. Int.*, 2004, **30**, p 2203–2209.
6. T. Shen, H. Xiong, Z. Li, L. Zhang, and K. Zhou, Fused Deposition Fabrication of High-Quality Zirconia Ceramics Using Granular Feedstock, *Ceram. Int.*, 2021, **47**, p 34352–34360.
7. R.H. Doremus and J.F. Shackelford, *Ceramic and Glass Materials: Structure*, Springer, Properties and Processing, 2008
8. G. Li, S. Tang, L. Yang, L. Qian, F. Liu, Z. Fan, K. Zuo, Q. Wei, and W. Jiang, Fabrication of Soluble Salt-Based Support for Suspended Ceramic Structure by Layered Extrusion Forming Method, *Mater. Des.*, 2019, **5**(183), p 108173.
9. B. Aktas, R. Das, A. Acikgoz, G. Demircan, S. Yalcin, H.G. Aktas, and M.V. Balak, DLP 3D Printing of TiO2-Doped Al2O3 Bioceramics: Manufacturing, Mechanical Properties, and Biological Evaluation, *Mater. Today Commun.*, 2024, **1**(38), p 107872.
10. P.F. Manicone, P.R. Iommetti, and L. Raffaelli, An Overview of Zirconia Ceramics: Basic Properties and Clinical Applications, *J. Dent.*, 2007, **35**(11), p 819–826.
11. B. Aktas and S. Tekeli, Effect of Co3O4 on the Fracture Toughness and Microstructure of Yttria-Stabilized Cubic Zirconia (8YSZ), *Acta Phys. Pol. A*, 2015, **127**, p 1384–1387.
12. J. Kelly and I. Denry, Stabilized Zirconia as a Structural Ceramic: An Overview, *Dent. Mater.*, 2008, **24**, p 289–298.
13. W. Qin, H. Majidi, J. Yun, and K. van Benthem, Electrode Effects on Microstructure Formation during Flash Sintering of Yttrium-Stabilized Zirconia, *J. Am. Ceram. Soc.*, 2016, **99**(7), p 2253–2259.

14. P. Arabkhani, H. Javadian, A. Asfaram, F. Sadeghfar, and F. Sadegh, Synthesis of Magnetic Tungsten Disulfide/Carbon Nanotubes Nanocomposite (WS2/Fe3O4/CNTs-NC) for Highly Efficient Ultrasound-Assisted Rapid Removal of Amaranth and Brilliant Blue FCF Hazardous Dyes, *J. Hazard. Mater.*, 2021, **15**(420), p 126644.
15. Y.-W. Chen, J. Moussi, J.L. Drury, and J.C. Wataha, Zirconia in Biomedical Applications, *Expert Rev. Med. Devices*, 2016, **13**, p 945–963.
16. L. Qian, L. Yang, G. Li, W. Jiang, and Z. Fan, Effect of Nano-TiO2 on Properties of 3 mol.% Yttria-Stabilized Zirconia Ceramic Via Layered Extrusion Forming, *J. Eur. Ceram. Soc.*, 2020, **40**, p 4539–4546.
17. D.-G. Ahn, Direct Metal Additive Manufacturing Processes and their Sustainable Applications for Green Technology: A Review, *Int. J. Precis. Eng. Manuf. Green Technol.*, 2016, **3**, p 381–395.
18. D. Grossin, A. Montón, P. Navarrete-Segado, E. Özmen, G. Urruth, F. Maury, D. Maury, C. Frances, M. Tourbin, P. Lenormand, and G. Bertrand, A Review of Additive Manufacturing of Ceramics by Powder Bed Selective Laser Processing (Sintering/Melting): Calcium Phosphate, Silicon Carbide, Zirconia, Alumina, and their Composites, *Open Ceram.*, 2021, **1**(5), p 100073.
19. I. Shishkovsky, I. Yadroitsev, P. Bertrand, and I. Smurov, Alumina-zirconium Ceramics Synthesis by Selective Laser Sintering/Melting, *Appl. Surf. Sci.*, 2007, **254**, p 966–970.
20. X. Guo, H. Yang, Y. Huang, and L. Zhang, Microstructure and Properties of Pore-Created SiC Ceramics with Calcium Chloride as Pore Former, *Ceram. Int.*, 2013, **39**, p 1299–1305.
21. J. Cai, S. Fan, F. Liu, W. Jiang, H. Wu, and Z. Fan, Preparation of Porous Al2O3 Ceramic Microspheres by a Novel Micro-Droplet Jetting Rapid Forming Method, *Ceram. Int.*, 2019, **45**, p 20583–20588.
22. Q. He, J. Jiang, X. Yang, L. Zhang, Z. Zhou, Y. Zhong, and Z. Shen, Additive Manufacturing of Dense Zirconia Ceramics by Fused Deposition Modeling Via Screw Extrusion, *J. Eur. Ceram. Soc.*, 2021, **41**, p 1033–1040.
23. T. Ayode Otitaju, P. Ugochukwu Okoye, G. Chen, Y. Li, M. Onyeka Okoye, and S. Li, Advanced Ceramic Components: Materials, Fabrication, and Applications, *J. Ind. Eng. Chem.*, 2020, **85**, p 34–65.
24. Y. Lakhdar, C. Tuck, J. Binner, A. Terry, and R. Goodridge, Additive Manufacturing of Advanced Ceramic Materials, *Prog. Mater. Sci.*, 2021, **1**(116), p 100736.
25. D. Nötzel and T. Hanemann, New Feedstock System for Fused Filament Fabrication of Sintered Alumina Parts, *Materials*, 2020, **13**(19), p 4461.
26. N. Furong, Y. Xiaole, L. Yuanbing, G. Jinyu, L. Peng, X. Zhipeng, and Y. Xianfeng, Fused Deposition Modeling of Si3N4 Ceramics: A cost-Effective 3D-Printing Route for Dense and high Performance Non-Oxide Ceramic Materials, *J. Eur. Ceram. Soc.*, 2022, **42**, p 7369–7376.
27. K. Rane and M. Strano, A Comprehensive Review of Extrusion-Based Additive Manufacturing Processes for Rapid Production of Metallic and Ceramic Parts, *Adv. Manuf.*, 2019, **7**, p 155–173.
28. P. Chen, X. Li, F. Tian, Z. Liu, D. Hu, T. Xie, Q. Liu, and J. Li, Fabrication, Microstructure, and Properties of 8 mol.% Yttria-Stabilized Zirconia (8YSZ) Transparent Ceramics, *J. Adv. Ceram.*, 2022, **11**, p 1153–1162.

**Publisher's Note** Springer Nature remains neutral with regard to jurisdictional claims in published maps and institutional affiliations.

Springer Nature or its licensor (e.g. a society or other partner) holds exclusive rights to this article under a publishing agreement with the author(s) or other rightsholder(s); author self-archiving of the accepted manuscript version of this article is solely governed by the terms of such publishing agreement and applicable law.